Fiber Bragg Grating Interrogation System Combining Wavelength-Swept Laser and Convolutional Neural Network

Tatsuya Yamaguchi, *Member, IEEE*, Hiroto Kawashima, Hiroki Matsuda, and Yukitaka Shinoda, *Member, IEEE*

***Abstract*—We propose a novel deep learning approach to improve the multipoint performance of fiber Bragg grating (FBG) interrogation systems with high-speed wavelength-swept lasers. Because conventional interrogation systems use wavelength-division multiplexing for multipointing FBGs, the number of FBGs is limited by the wavelength bandwidth of the light source. To overcome this, we attempted to improve the multipoint performance of wavelength-division multiplexing by using multiple FBGs of the same wavelength. However, it is difficult to analyze the peak wavelengths of individual FBGs using a high-speed wavelength-swept laser because the optical spectra of FBGs at the same wavelength are observed to occur in a complex overlapping manner on the microsecond order. Here, we present a peak-detection method based on a convolutional neural network (CNN) in deep learning as a breakthrough in solving this problem. The experiment combines a high-speed wavelength-swept laser and a CNN to achieve high-speed measurement of three overlapping FBGs at the same wavelength. The results demonstrate that a measurement rate of 50 kHz and a wavelength resolution of 4.2 pm can be achieved, improving the limit of wavelength-division multiplexing by a factor of three. Our approach is to simply incorporate peak detection with CNN into existing wavelength-swept laser-based interrogators, which can function as if they were interrogators with several times the multipoint performance.**

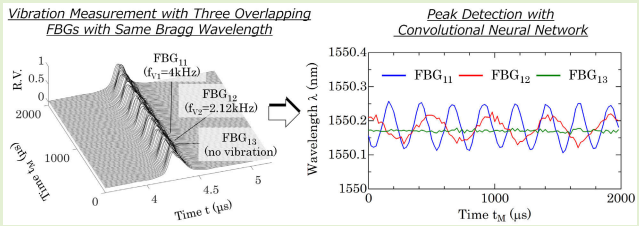

***Index Terms*— Convolutional neural networks (CNNs), deep learning, fiber Bragg gratings (FBGs), optical fiber sensors, wavelength-swept lasers.**

I. Introduction

FIBER Bragg gratings (FBGs) in optical fiber sensors have been the subject of extensive research over the past several decades owing to their excellent properties, including low weight, corrosion resistance, and electrical insulation [1], [2], [3]. Currently, advances in sensing technology have been expanding their use to a wide range of areas, including energy, environmental monitoring, and aerospace [4], [5], [6]. An FBG is made by forming periodic refractive-index variations in the core of an optical fiber and reflects light only in a specific wavelength region called the Bragg wavelength. The Bragg wavelength is sensitive to various physical quantities such as strain and temperature, allowing FBGs to be used to measure various parameters [7], [8], [9], [10]. Through the fabrication of multiple FBGs within a single optical fiber, a variety of parameters can be observed simultaneously.

Various measurement approaches have been vigorously studied to maximize the potential of FBGs as sensors. These include typical methods such as spectroscopy, interferometry, and wavelength sweep [2], [11], [12], [13]. Each method has its advantages and disadvantages; however, the wavelength-sweep method [13] is characterized by its ability to perform both high-speed and multipoint measurements. The measurements are performed using a wavelength-swept laser, which encodes the FBG reflection wavelength information as reflection time information. The measurement speed is determined by the sweep rate of the wavelength-swept laser. Therefore, high-speed wavelength-swept lasers with Fourier-domain mode locking (FDML) and buffer optics developed for medical imaging have been converted for FBG measurement, enabling measurement rates to exceed several tens of kilohertz [14],

Manuscript received 5 April 2024; revised 20 May 2024; accepted 25 May 2024. Date of publication 5 June 2024; date of current version 16 July 2024. This work was supported in part by the Japan Society for the Promotion of Science (JSPS) KAKENHI under Grant 20K14754 and Grant 24K17288 and in part by the Nihon University College of Science and Technology for Research. The associate editor coordinating the review of this article and approving it for publication was Prof. Arnaldo Gomes Leal-Junior. *(Corresponding author: Tatsuya Yamaguchi.)*

Tatsuya Yamaguchi and Yukitaka Shinoda are with the Department of Electrical Engineering, College of Science and Technology, Nihon University, Tokyo 1010062, Japan (e-mail: yamaguchi.tatsuya@nihon-u.ac.jp; shinoda.yukitaka@nihon-u.ac.jp).

Hiroto Kawashima and Hiroki Matsuda are with the Department of Electrical Engineering, Graduate School of Science and Technology, Nihon University, Tokyo 1010062, Japan (e-mail: cshi22013@g.nihon-u.ac.jp; cshi22035@g.nihon-u.ac.jp).

Digital Object Identifier 10.1109/JSEN.2024.3407359

[15], [16], [17], [18], [19]. Multipoint measurements are made using wavelength-division multiplexing, with each FBG assigned a unique occupied wavelength range. Therefore, the number of FBGs installed is limited by the wavelength range of the light source, making the development of novel multipoint technologies essential. Although various optical approaches, such as the use of interferometers [20], [21], [22], have been proposed, it remains difficult to achieve multipoint measurements without sacrificing performance in terms of sensitivity, measurement speed, and cost.

Herein, we propose a novel method that uses deep learning to improve the multipoint performance of the wavelength-sweep method several times without changing the hardware in any way. This method first multiplexes using FBGs at the same wavelength to improve the performance of wavelength-division multiplexing. However, in a high-speed wavelength-swept laser, the optical spectra of FBGs at the same wavelength overlap in a complex manner and are observed with a period on the order of microseconds. This makes it difficult to analyze the peak wavelengths of individual FBGs using conventional peak-detection techniques such as maximum value detection and center-of-gravity detection. Therefore, we have devised a peak-detection method based on a convolutional neural network (CNN) with deep learning to be adapted for wavelength-sweep methods as a breakthrough in solving this problem.

Peak-detection methods that use deep learning have been extensively studied for FBG measurements that are based on the use of spectroscopy [23], [24], [25], [26], [27], [28]. Deep learning, with its high feature extraction capability, learns the unique spectral information of FBGs as features and enables tracking of the peak wavelength of a specific FBG. Many studies have assigned a unique full width at half maximum (FWHM) or reflectance to individual FBGs at the same wavelength to facilitate identification by deep learning. Deep learning has been reported to achieve a picometer resolution. Our previous work [27], [28] proposed a method based on data augmentation called noise-additive learning [29], [30]. This method effectively reinforces the tolerance of machine learning to variations in experimental signals. The results demonstrate that complex overlap problems with multiple FBGs that vary at arbitrary wavelengths can be analyzed with a picometer resolution. To date, peak detection has been demonstrated only for spectroscopic methods. The spectroscopy method [2], [23], [24], [25], [26], [27], [28] uses an optical spectrum analyzer, which limits the measurement rate to a few hundred hertz at most. Although an increase in the measurement rate is required for vibration detection, which is the main application of FBGs, to the best of our knowledge, no breakthroughs have been achieved thus far. Therefore, we promote research on deep learning that can be adapted to the wavelength-sweep method to significantly improve its measurement rate.

In the experiment, an FDML laser [17], [18] with a sweep rate of 50 kHz was used to acquire the reflected signals of overlapping FBGs of the same wavelength at a high speed. A CNN is a powerful method for extracting unique features using convolutional filters, and its accuracy has been reported to be high, particularly in medical image analysis and automatic driving [31], [32]. Experiments were successfully performed to analyze three FBGs multipointed with the same wavelength with a wavelength resolution of 4.2 pm. The results demonstrated a threefold improvement in the multipoint performance of wavelength-division multiplexing. This method requires only the incorporation of a CNN-based peak-detection process and is expected to significantly improve multipoint performance at a low cost without compromising the performance of the wavelength-sweep method. The experiments successfully achieved a measurement rate of 50 kHz, which is nearly two orders of magnitude higher than that of the spectroscopy method. This revealed that FBGs with the same wavelength can be used for vibration measurements beyond a few kilohertz. To the best of our knowledge, these results represent the fastest measurement rates among those reported in studies on FBG measurements at the same wavelength based on the use of deep learning.

II. Experimental Setup

A. FBG Interrogation System With FDML Laser and CNN

Fig. 1 shows the proposed FBG interrogation system, which combines an FDML laser and a CNN. The FDML laser is controlled by a sinusoidal sweep signal, V_S, output by an oscillator. FDML is a well-known method for the high-speed operation of fiber ring lasers [14]. This method synchronizes the light's orbit time in the fiber ring resonator with the wavelength filter drive's period. The FDML laser operates with a center wavelength of 1552.4 nm, sweep bandwidth of 1542.7–1562.2 nm, sweep rate f_m of 50 kHz, and sweep period T_m $(= 1/f_m)$ of 20 μs [17], [18]. The output light from the FDML laser is amplified by an optical amplifier (SOA1013, Thorlabs) and then injected into a fiber switch. The fiber switch (NSSW, Agiltron) has a repetition rate of dc to 500 kHz and an on–off ratio of ~39 dB. The fiber switch is controlled by the pulse signal, V_P, with the oscillator with a pulsewidth t_{PW} ~9 μs $(\sim 1/2 f_m)$ to extract the light swept in the long-wavelength direction of the FDML laser. The extracted light then enters the multipoint FBG sensor via a circulator.

The interrogation system is equipped with six FBGs of the same and different wavelengths in three bifurcated optical paths. FBG_{1j} $(j = 1, 2, 3)$ has a Bragg wavelength λ_{B_1j} of 1550 nm; FWHM $\Delta\lambda_{B\_1j}$ of 0.2, 0.4, and 0.7 nm, respectively; and a reflectivity of approximately 3%. FBG_{2j} $(j = 1, 2, 3)$ has a Bragg wavelength λ_{B_2j} of 1555 nm; FWHM $\Delta\lambda_{B\_2j}$ of 0.2, 0.4, and 0.7 nm, respectively; and a reflectivity of approximately 3%. Each FBG at the same wavelength is assigned a unique FWHM characteristic to facilitate its identification by the CNN. The light reflected from each FBG is combined with a coupler and received by a detector (P6713, Tektronix) via a circulator. The detector signal, V_D, is collected by an analog-to-digital converter (NI PXIe-5170R, National Instruments) with a sampling frequency of 250 MHz and 14-bit resolution. The collected signal comprises those from the FBGs of the same wavelength and of different wavelengths, which are observed to occur in a complex overlapping manner. To detect the peak signals of the individual FBGs at a high temporal resolution, a peak-detection process based

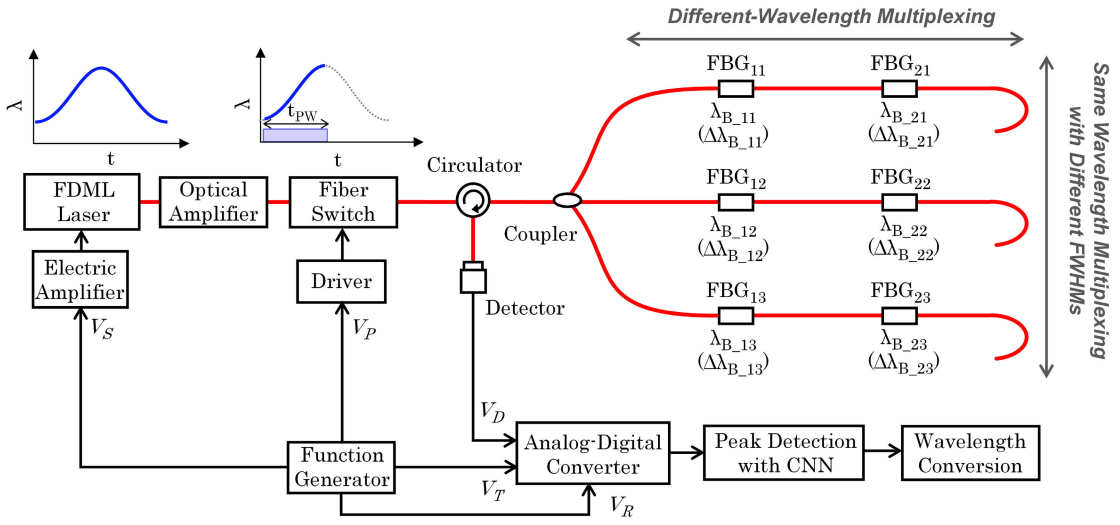

Fig. 1. FBG Interrogation system combining FDML laser and CNN. V_S—sweep signal; V_P—pulse signal; V_D—detector signal; V_T—trigger signal; and V_R—reference clock signal.

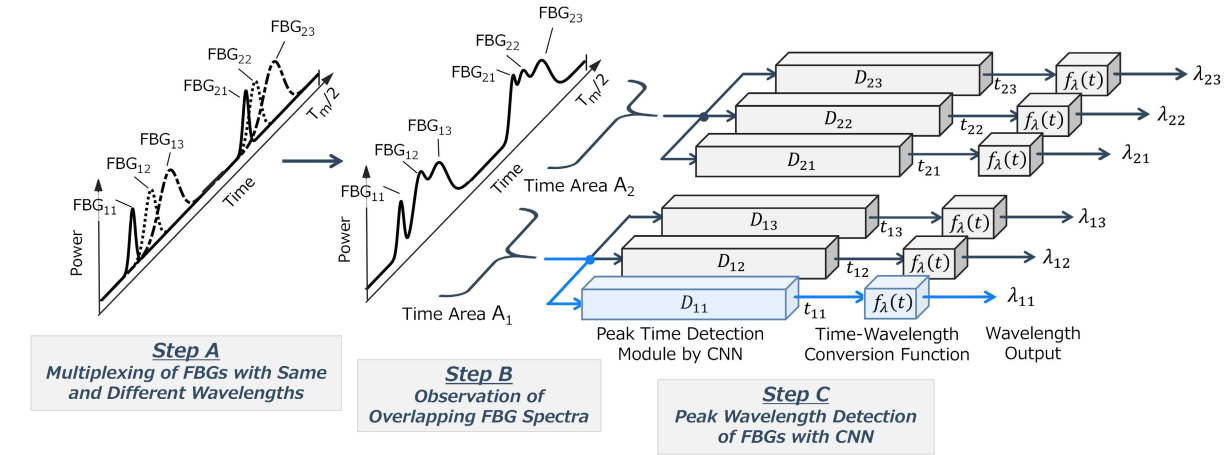

(a)

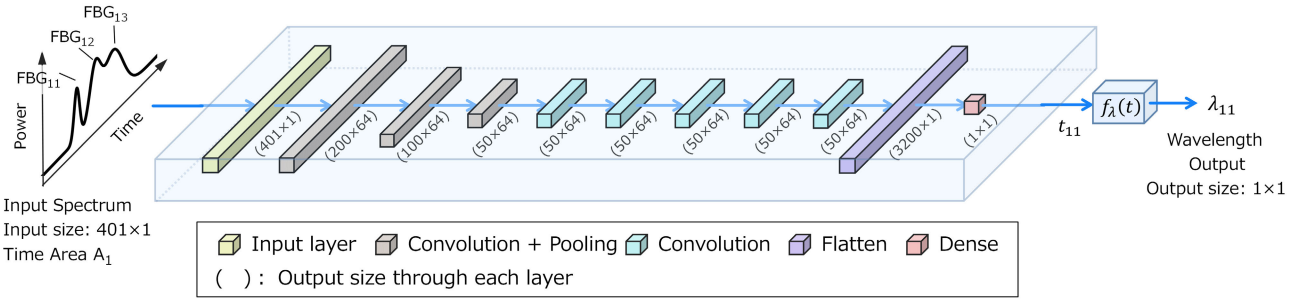

(b)

Fig. 2. Concept of peak wavelength detection with CNN. (a) Module setup for measuring FBGs. (b) Layer design of peak-detection module D_{11} with CNN for FBG_{11}.

on the use of a CNN is implemented. In the wavelength-sweep method, information on the peak wavelength of each FBG is observed as the peak time information. Therefore, a time–wavelength conversion formula was derived based on the sweep characteristics of the laser, which have been outlined in Section III-A. In the experiment, the peak time of each FBG was detected using the CNN at a measurement rate of 50 kHz ($= 1/f_m$) and converted to its corresponding wavelength.

B. Peak-Detection Processing With CNN

Fig. 2 shows the proposed peak-detection process based on the use of a CNN. As shown in Fig. 2(a), when FBG_{1j} and FBG_{2j} are multipointed using a wavelength-swept laser, the FBG signals can be observed to overlap in the time domain, making it difficult to analyze the peak times of individual FBGs using conventional peak-detection techniques. To solve this problem, first, FBG_{1j} and FBG_{2j} with different

wavelengths are divided into time areas A_1 and A_2 to divide them in the time domain. Each area after segmentation contains the peak signals of three overlapping FBGs of the same wavelength, which can then be detected using the proposed CNN-based method. The proposed peak-detection method consists of six modules D_{1j} and D_{2j}, corresponding to FBG_{1j} and FBG_{2j}, respectively. The six modules D_{1j} and D_{2j} are optimized to detect the peak times t_{1j} and t_{2j}, respectively, of each FBG using the learning method described later. The detected peak times t_{1j} and t_{2j} are converted to wavelengths λ_{1j} and λ_{2j}, respectively, using the wavelength conversion formula $f_\lambda(t)$ based on the sweep characteristics of the laser.

Fig. 2(b) shows the inside of the peak-detection module D_{11} of FBG_{11} composed of a CNN. The internal network is composed of multiple layers with different roles. The input signal is the time area A_1 where FBG_{1j} is observed. A_1 has a time range of $t = 3.6$–5.2 μs and 401 data points (see Section III-B). The input signal is passed to the input layer of D_{11}. The input signal is then input into the convolution layer. The convolution layer performs convolution operations using a convolution filter to extract the feature data from the input signal. The size of the filters is 5×1, the activation function is a nonlinear ReLU, the number of filters is 64, and padding is applied. The extracted feature data are input into the pooling layer, which compresses and aggregates large amounts of feature data. The pooling method used is averaging, and the pooling size is 2×1. A pooling layer is placed after the convolution layer to aggregate the extracted features. These two layers are multilayered to efficiently collect the important features of FBG_{11}. The network consists of eight convolutional layers and three pooling layers. The eighth convolution layer outputs the aggregated 2-D feature data (50×64), which are input into the flatten layer. The flatten layer serves as a preprocessing step to input the feature data into the final stage, which is the dense layer. The flatten layer converts the data into 1-D data (3200×1). The converted 1-D feature data are combined into a single point in the dense layer. The flatten and dense layers are combined using optimized weights, and the feature data are converted to the peak time t_{11}. The other FBG modules also constitute a network similar to the module D_{11} of FBG_{11}. The CNN was developed in MATLAB (Mathworks) using a computer with a Core i7-9800X CPU, NVIDIA GeForce3070TI, and 32 GB of RAM.

III. Experimental Results

A. Characteristics of FDML Laser and Multipoint FBGs

Fig. 3 shows the optical spectrum of the FDML laser obtained using an optical spectrum analyzer. An optical spectrum analyzer (AQ6317B, Ando) was set to an average frequency of 10. The FDML laser operated at a sweep rate of $f_m = 50$ kHz and emits light in the 1.55-μm wavelength band. The FDML laser had a center wavelength of 1552.4 nm and a sweep bandwidth of 1542.7–1562.2 nm.

The sweep characteristics of the FDML laser were then evaluated. A tunable filter (FFM-C, Axsun Technologies) was used to extract light only in a specific wavelength region of the FDML laser. The extracted light was analyzed using a detector and wavelength monitor (FB200, Ando) to

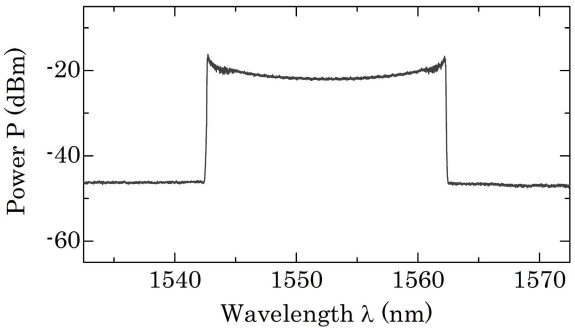

Fig. 3. Output spectrum of FDML laser.

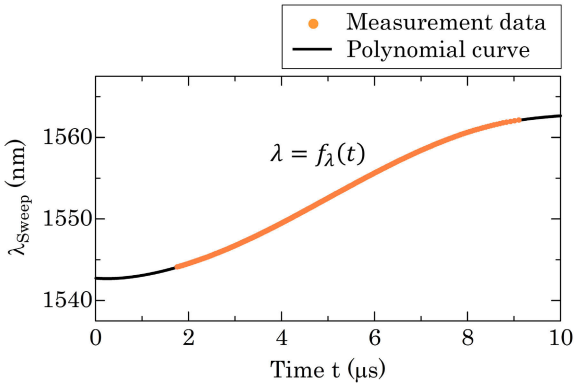

Fig. 4. Sweep characteristics of FDML laser.

evaluate the relationship between time and wavelength. The wavelength monitor has a wavelength resolution of 1 pm, measurement accuracy of ± 50 pm, and wavelength range of 1527–1567 nm. The number of measurement points was set to 250. Fig. 4 shows the sweep characteristics of the FDML laser. The FDML laser swept the oscillation wavelength sinusoidally in the wavelength range 1542.7–1562.2 nm. The time–wavelength conversion formula $f_\lambda(t)$ was derived by applying a polynomial approximation to the obtained sweep characteristics of the FDML laser.

The FDML laser was used to measure the signals reflected from the FBGs. A portion of the output light of the FDML laser was extracted by a fiber switch operating at a pulsewidth of $t_{\mathrm{PW}} \sim 9$ μs. FBG_{1j} were subjected to strain $\Delta\varepsilon_{1j} = 500$ $\mu\varepsilon$, respectively. FBG_{21} was kept strain-free, whereas FBG_{22} and FBG_{23} were subjected to strain $\Delta\varepsilon_{22} = 500$ $\mu\varepsilon$ and $\Delta\varepsilon_{23} = 500$ $\mu\varepsilon$, respectively. Fig. 5 shows the detected reflected signals from the FBGs. Fig. 5(a) shows the extracted light of the FDML laser. The extracted light had a pulsewidth $t_{\mathrm{PW}} \sim 9$ μs and was repeatedly output with a sweep period $T_m = 20$ μs. Fig. 5(b) shows the signals reflected from the FBGs using the laser. The signals of FBG_{1j} (1550 nm) and FBG_{2j} (1555 nm) at the same wavelength were detected to be overlapping each other at approximately 4.4 and 6.0 μs, respectively.

B. Creation of FBG Numerical Model

CNNs can improve peak-detection performance by using more than tens of thousands of points of training data. The training data should include overlapping FBG signals

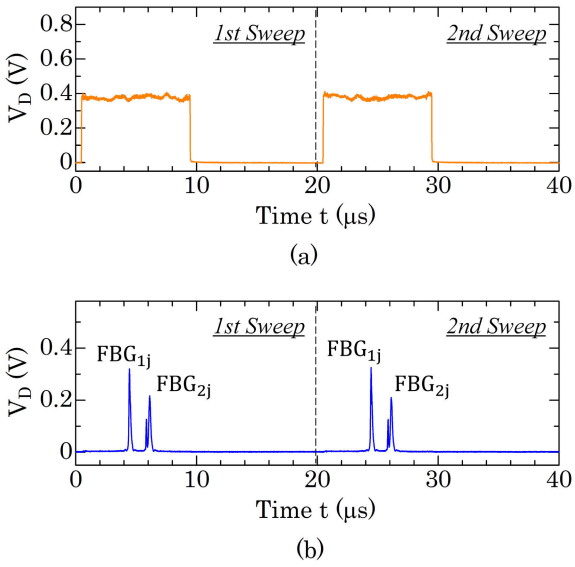

Fig. 5. Detector signal of FBGs with laser sweep. (a) Laser output. (b) FBGs.

under various conditions. However, it is impractical to collect large amounts of training data during an experiment. This section describes a numerical model of an FBG using a Gaussian approximation for the efficient generation of training data.

Fig. 6(I) shows the experimentally observed reflection signal at FBG_{2j} (1555 nm). FBG_{21} was set to be strain-free, FBG_{22} was subjected to $\Delta\varepsilon_{22} = 500\ \mu\varepsilon$, and FBG_{23} was subjected to $\Delta\varepsilon_{23} = 500\ \mu\varepsilon$. Fig. 6(I-a)–(I-c) shows the results of independent observations on FBG_{21} ($\Delta\lambda_{B\_21} = 0.2$ nm), FBG_{22} ($\Delta\lambda_{B\_22} = 0.4$ nm), and FBG_{23} ($\Delta\lambda_{B\_23} = 0.7$ nm), respectively. The signals reflected from each FBG with different FWHMs were observed. Fig. 6(I-d) shows the results of the simultaneous observation of all FBGs, where the signals reflected from the FBGs were observed to overlap each other. The following Gaussian approximation [25], [27], [28] was applied to Fig. 6(I-a)–6(I-c) to create a numerical model of the FBG

$$R_{ij}\left(t, t_{B\_ij}\right) = I_{\text{peak}\_ij} \exp\left[-4\ln 2\left(\frac{t - t_{B\_ij}}{\Delta t_{B\_ij}}\right)^2\right] \quad (1)$$

where $i = 1, 2$; $j = 1, 2, 3$; I_{peak_ij} is the intensity of the FBG; t_{B_ij} is the peak time with the Bragg wavelength of the FBG; Δt_{B_ij} is the FWHM of the FBG in the time domain; i is the address in the wavelength-multiplexing direction of the FBG, and j is the address in the FWHM-multiplexing direction of the FBG.

Fig. 6(II-a)–(II-c) shows the results of the numerical models for FBG_{21}, FBG_{22}, and FBG_{23}, respectively. The numerical models for each FBG were in good agreement with the experimental reflection signals shown in Fig. 6(I-a)–(I-c). Fig. 6(II-d) shows the results of adding the numerical models for each FBG. The numerical model results in Fig. 6(II-d) well reproduced the experimentally observed FBG signal in Fig. 6(I-d). The numerical model for FBG_{1j} (1550 nm) was created in a similar manner.

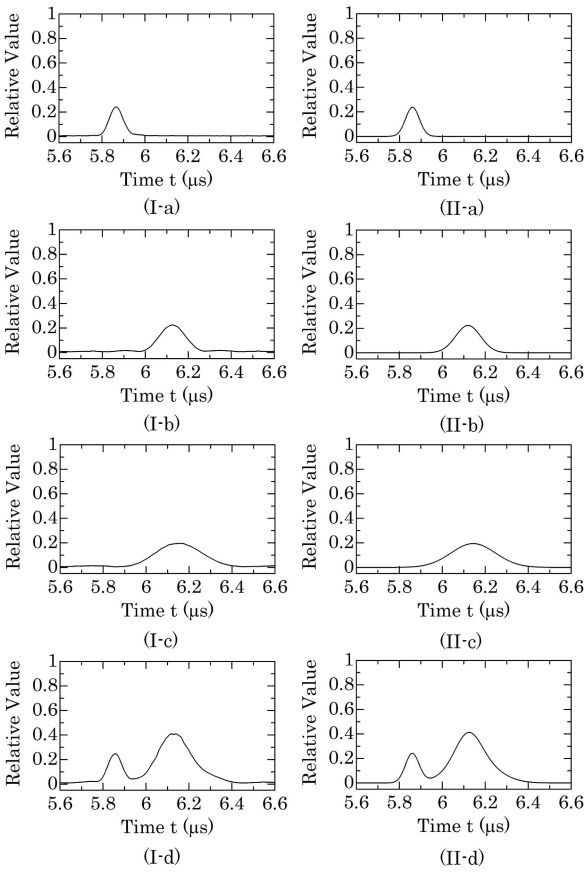

Fig. 6. Numerical modeling using Gaussian approximation. (I) Experimental results. (II) Numerical models. (a) FBG_{21}. (b) FBG_{22}. (c) FBG_{23}. (d) Multiplexed FBGs.

C. CNN Training for Peak Detection

Numerical models were used to generate training data and to train the CNN for peak detection. The analysis time ranges A_1 and A_2 for FBG_{1j} and FBG_{2j} were $t = 3.6$–$5.2\ \mu$s and $t = 5.2$–$6.8\ \mu$s, respectively. The number of data points in A_1 and A_2 was 401. A total of 226 981 training data points were generated under various overlapping conditions by adjusting t_{B_ij} in the numerical model of (1) for each FBG. Our CNN was developed using a deep learning toolbox for training and a parallel computing toolbox for GPU processing in the MATLAB environment. Training does not require the extensive collection of experimental data because only the dataset generated by the numerical model was used. Nevertheless, our CNN revealed that peak wavelength detection could be achieved with picometer resolution. The optimization algorithm used for learning was the Adam algorithm. The initial learning ratio was set at 0.001. In the case of training the peak-detection module D_{11} of FBG_{11} shown in Fig. 2, the overlapping signals of FBG_{1j} with the analysis time range A_1 were selected as explanatory variables, and the peak time t_{B_11} of FBG_{11} was selected as the objective variable. Conventional CNNs trained only with numerical models have a problem with reduced tolerance to experimental signal variations, resulting in a decrease in the accuracy of peak detection. This is caused by the gap between the smooth numerical model and noisy experimental signal, as shown in Fig. 6. The experiment

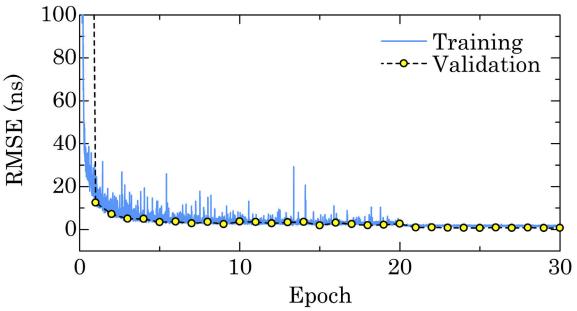

Fig. 7. Variation of RMSE with number of epochs.

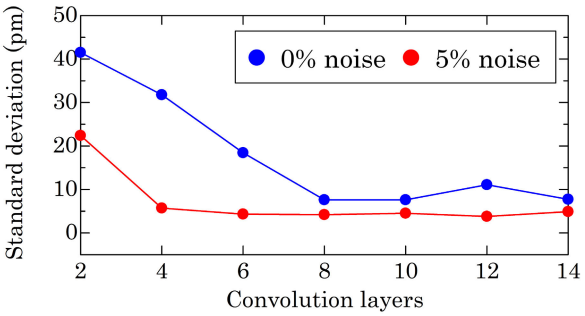

Fig. 8. Standard deviation for peak-wavelength measurement with respect to number of convolution layers.

introduced noise-additive learning for data augmentation [27], [28]. Noise-additive learning adds normalized noise to the training data. The noise was set to 5% of the FBG signal amplitude.

First, the root-mean-square error (RMSE) [25], [27] was calculated using the following equation to evaluate the peak-detection performance of the developed CNN:

$$\mathrm{RMSE} = \sqrt{\frac{\sum_{i=1}^{n}\sum_{j=1}^{m}\left(t_{B\_ij} - t_{ij}\right)^2}{n \times m}} \tag{2}$$

where $n = 2$; $m = 3$; and t_{ij} is the peak time at Bragg wavelength predicted by the CNN.

Fig. 7 shows the training results of the CNN. The CNN had eight convolutional layers. The horizontal axis represents the number of epochs, indicating the number of learning iterations, and the vertical axis represents the RMSE. A numerical model was used to generate the training and validation data, resulting in a total of 226 981 data points. The number of epochs indicates the degree to which learning has progressed. One epoch refers to the degree of training progress using the dataset once. The CNN exhibited decreasing RMSE as learning progressed. At 30 epochs, the RMSE of the verification data was 0.74 ns, which is well below the sampling time of 4 ns of the analog-to-digital converter. This indicates that the CNN is effective at detecting peaks with a high temporal resolution. The FDML laser had a sweep period of 20 μs and a sweep bandwidth of approximately 20 nm. Therefore, the RMSE of the wavelength based on the peak time detection by the CNN was estimated to be ~2.3 pm.

The CNN-based peak-detection process was then adapted to the experimentally observed FBG reflection signal. The peak time t_{ij} of the detected FBG_{ij} was converted to the peak wavelength λ_{ij} using the wavelength conversion formula $f_\lambda(t)$. For each FBG, the strain was kept constant, the number of measurement points was 100, and the standard deviation of the peak wavelength was calculated. In addition, to improve the peak-detection performance of the CNN, the number of convolutional layers and the presence of noise-additive learning were examined. Fig. 8 shows the standard deviations of the peak-wavelength measurements using the CNN. Without noise-additive learning, the standard deviations were 41.5 pm for two layers and 7.6 pm for eight layers, with the standard deviation improving with the number of convolutional layers. Increasing the number of convolutional layers in CNNs is effective for representing more complex models. However, CNNs trained only with numerical models had lower measurement accuracies owing to the effect of experimental signal variation. By contrast, with 5% noise-additive learning, the results improved to 22.4 pm for two layers and 4.2 pm for eight layers. After eight layers, the standard deviation remained constant at ~4 pm. Based on the aforementioned results, the subsequent experiment applied noise-additive learning and employed a CNN with eight convolutional layers to analyze the peak wavelengths of the FBGs.

D. Measurement in Static-Strain Conditions

In this experiment, the simultaneous measurement of FBG_{1j} (1550 nm) and FBG_{2j} (1555 nm) was verified by combining same-wavelength multiplexing and wavelength-division multiplexing. Fig. 9(I-a) and (II-a) shows the experimental conditions in terms of strain applied to each FBG. The applied range of strain was 0–1000 $\mu\varepsilon$ and the number of measurement points was 43. FBG_{21} was assumed to be strain-free. Fig. 9(I-b) and (II-b) shows the reflected signals of FBG_{1j} and FBG_{2j}. Each FBG reflection signal was observed to have a shifted peak time according to the respective strain conditions. However, it is not easy to analyze the peak times of individual FBGs, because the reflected signals of multiple FBGs overlap. Fig. 9(I-c) and (II-c) shows the results of the peak-wavelength measurement of FBG_{1j} and FBG_{2j} based on the use of a CNN without noise-additive learning. Changes in the individual peak wavelengths of FBG_{1j} and FBG_{2j} in different wavelength regions could be detected. However, the linearity of the peak detection with respect to the strain was reduced owing to variations in the experimental signal caused by the experimental system. Fig. 9(I-d) and (II-d) shows the results of peak detection using a CNN with 5% noise-additive learning. The linearity improved at each FBG peak wavelength. The peak-wavelength changes $\Delta\lambda_{11}$, $\Delta\lambda_{12}$, and $\Delta\lambda_{13}$ of FBG_{1j} for 1000 $\mu\varepsilon$ of strain were approximately 1.17, 1.17, and 1.16 nm, respectively, and the peak-wavelength changes $\Delta\lambda_{22}$ and $\Delta\lambda_{23}$ of FBG_{2j} were approximately 1.15 and 1.20 nm, respectively. The measurement of three same-wavelength FBGs in wavelength-division multiplexing was achieved, demonstrating that the limits of wavelength-division multiplexing could be improved by a factor of three.

To verify in detail the effectiveness of CNN peak detection with noise-additive learning, the linearity of peak

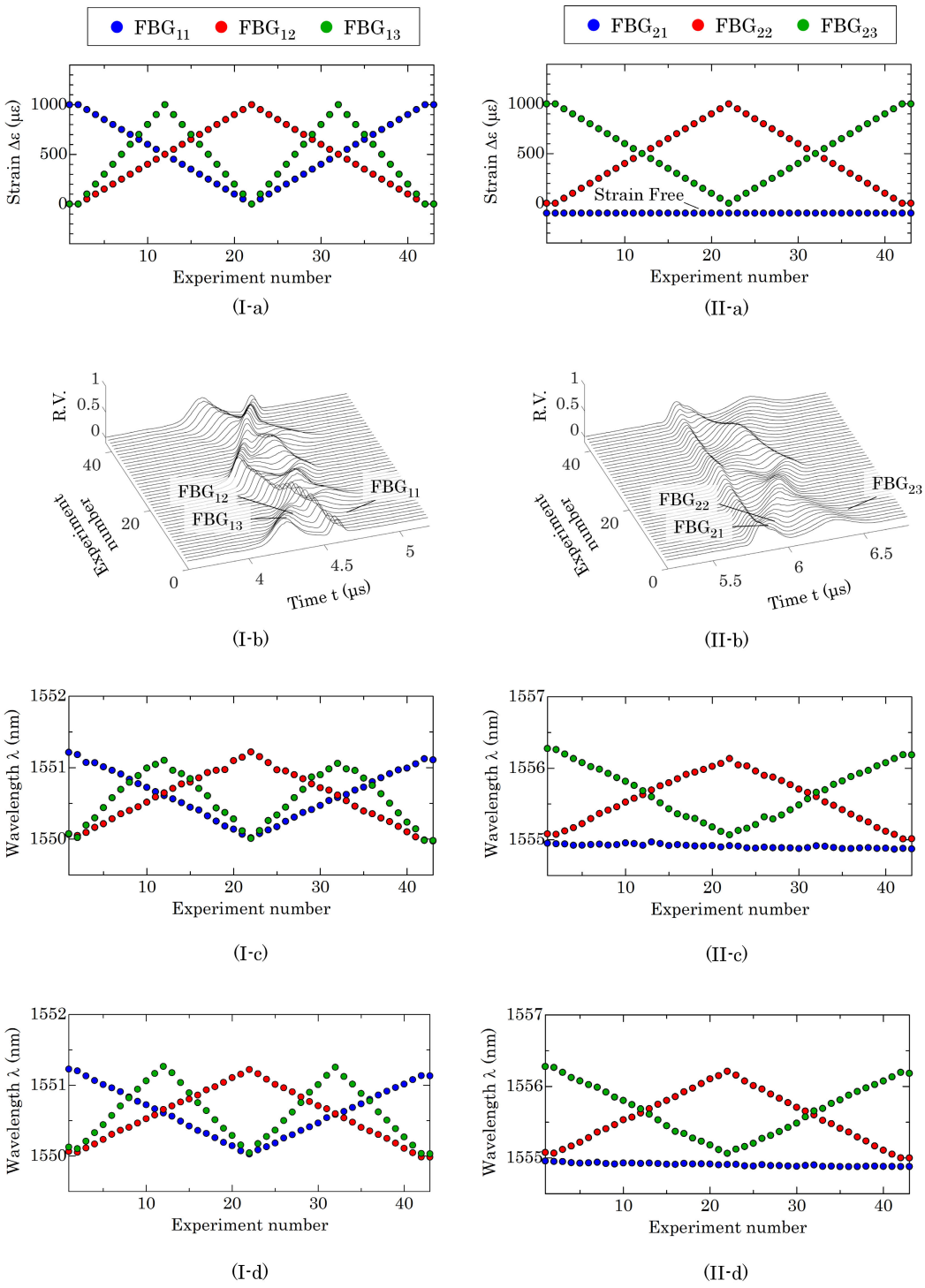

Fig. 9. Strain measurements of multiplexed FBGs combining same and different wavelengths. (I) FBG_{11}, FBG_{12}, and FBG_{13}. (II) FBG_{21}, FBG_{22}, and FBG_{23}. (a) Strain condition. (b) Spectra of three FBGs. (c) Peak wavelengths obtained using CNN without noise-additive learning. (d) Peak wavelengths obtained using CNN with noise-additive learning.

detection for FBG_{13} was evaluated. In the evaluation, a CNN with noise-additive learning with a noise-ratio range of 0%–20% was used and adapted for the results shown in Fig. 9(I-b). Fig. 10(a) shows the results for the slope of FBG_{13} with respect to the noise ratio for noise-additive learning. The slopes were approximately 1.09 pm/$\mu\varepsilon$ for 0% noise, i.e., without noise-additive learning, and approximately 1.19 pm/$\mu\varepsilon$ for 5% noise. The strain characteristics of FBG_{13} alone were evaluated using a wavelength monitor (FB200, Ando), resulting in a slope of approximately 1.19 pm/$\mu\varepsilon$. This was in good agreement with the results of noise-additive learning with 5% noise. The slope was approximately constant for noise above 5%. Fig. 10(b) shows the results for the coefficient of determination of FBG_{13} with respect to the noise ratio for

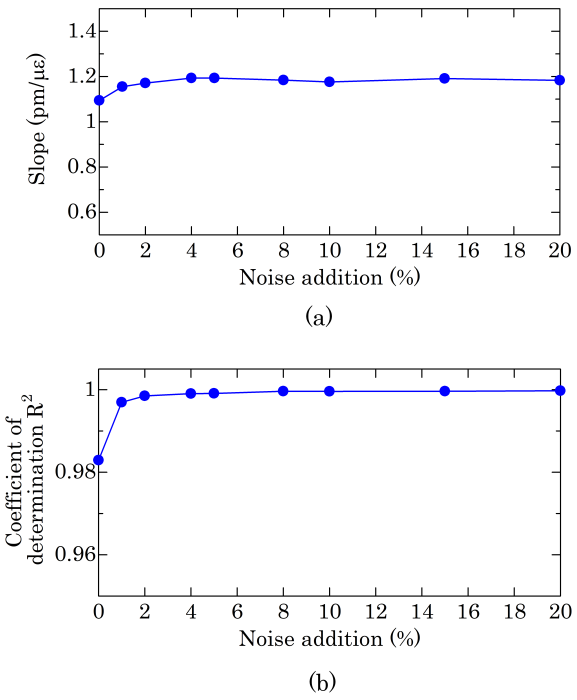

Fig. 10. Evaluation of linearity of FBG_{13} for CNN trained with noise addition. (a) Slope. (b) Coefficient of determination.

noise-additive learning. The coefficients of determination were 0.9829 for 0% noise and 0.9991 for 5% noise. The values were approximately constant for noise ratios above 5%. The experiments revealed that noise-additive learning improves the linearity of peak detection. In subsequent experiments, a CNN with 5% noise-additive learning was used.

E. High-Speed Vibration Measurement

The interrogation system, which combined an FDML laser and a CNN, was used to verify high-speed vibration measurements using FBG_{1j} at the same wavelength. The FDML laser was set to a sweep rate of 50 kHz, sweep number of 100, and measurement time of 2000 μs. Piezoelectric transducers were installed in FBG_{11} and FBG_{12}, and the vibration frequencies f_{v1} and f_{v2} were set to 4 and 2.12 kHz, respectively. Fig. 11(a) shows the reflected signal of FBG_{1j}. Although it could be confirmed that the signals of overlapping FBGs were periodically shifted, it was not easy to identify and analyze which FBGs were subjected to vibration. Fig. 11(b) shows the results of the peak-wavelength measurement based on the use of a CNN. The CNN clearly tracked the periodic peak wavelength changes at each vibration frequency applied to FBG_{11} and FBG_{12}. The peak-to-peak wavelength values due to vibration in FBG_{11} and FBG_{12} were approximately 0.15 and 0.10 nm, respectively. Despite the complex overlapping of the FBG signals in the experiment, the peak wavelength of FBG_{13} was barely affected by the vibrations of the other FBGs. This suggests that the powerful feature extraction function of the CNN is effective at identifying the signal of each FBG and is able to detect the peak wavelength of each FBG. The interrogation system used an FDML laser with a sweep rate of 50 kHz and was able to measure the peak wavelength of

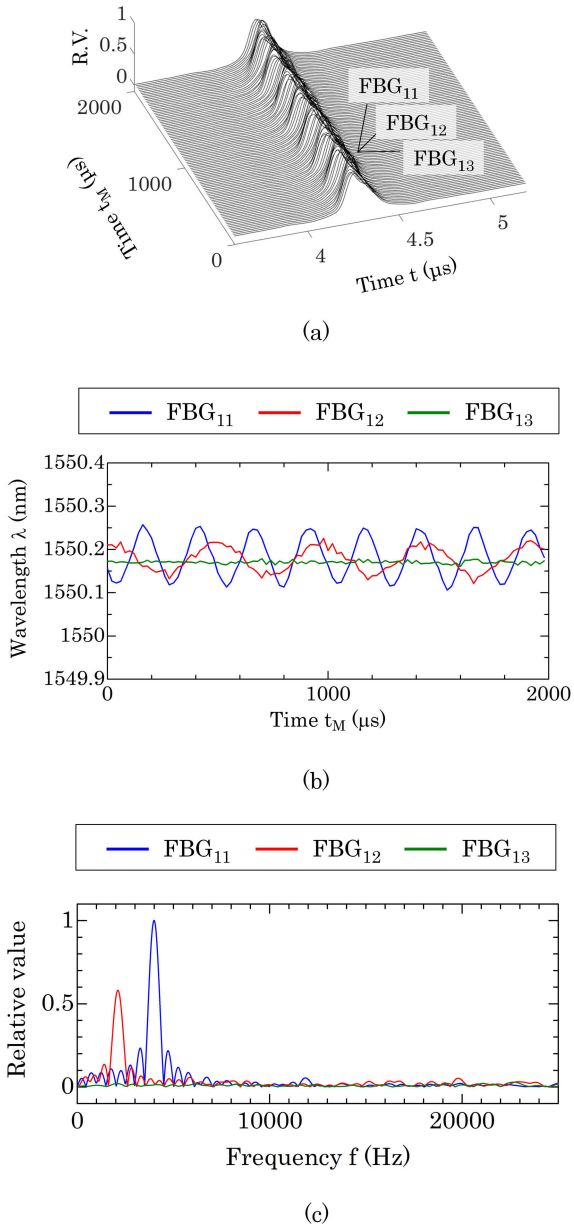

Fig. 11. Simultaneous vibration measurements of different vibrating elements attached to FBG_{11} and FBG_{12}. (a) Spectra of three FBGs. (b) Peak wavelengths of each FBG. (c) Frequency analysis.

each FBG with a temporal resolution of 20 μs. Fig. 11(c) presents the results of frequency analysis on the results shown in Fig. 11(b). To increase the analytical resolution of the frequency analysis, 3996 zero paddings were applied to the 100 experimental data points obtained, thus expanding them to 4096 data points. In the frequency analysis, steep frequency spectra were observed for FBG_{11} and FBG_{12} at the applied vibrational frequency. The frequencies of maximum amplitude were 3.99 and 2.11 kHz, respectively, and each FBG was able to measure the vibration frequency. Frequency analysis results showed that vibration frequencies applied to certain FBGs were not detected by other FBGs. This indicates that the CNN models for each FBG operate independently of each other and clearly detect the peak wavelength of a particular

FBG. The results demonstrated that the proposed interrogation system, which combined an FDML laser and a CNN, could achieve high-speed vibration measurements using multiplexed FBGs at the same wavelength.

IV. Conclusion

In this study, we developed an interrogation system that combined an FDML laser and a CNN. The system was capable of measuring, simultaneously and at high speed, three FBGs multiplexed at the same wavelength. The results showed that the limit of wavelength-division multiplexing could be improved by a factor of three at a measurement rate of 50 kHz and a wavelength resolution of 4.2 pm. Consequently, the wavelength-sweep method with the proposed approach succeeded in accelerating the measurement rate by approximately two orders of magnitude higher than those of spectroscopy methods developed in past studies. The higher measurement rate revealed that FBGs of the same wavelength can be adapted for vibration measurements. These findings allow existing wavelength-swept laser-based systems to simply incorporate CNNs and function as if they can produce a several times better multipoint performance without any hardware changes.

Future research studies are expected to combine faster wavelength-swept lasers with CNNs to improve measurement time resolution. It is clear that CNNs can analyze FBGs at the same wavelength using wavelength-swept lasers; however, further work is required to improve and develop the network to achieve further multiplexing of FBGs. Our CNN assigns unique FWHMs to FBGs of the same wavelength to facilitate the identification of FBGs. To multipoint more FBGs, the FBGs must be arranged with the FWHMs shifted as slightly as possible. In addition, a key challenge is developing a high-performance machine learning model that can identify this slight FWHM difference in FBGs. Further multipointing of FBGs will require machine learning models that can tolerate more complex spectral overlaps because of the increased number of sensors. A simple approach would be to significantly improve the number of datasets; however, this could inflate the computational cost. Therefore, machine learning models that can learn effectively with smaller datasets must be developed. By increasing the speed of the sweep rate of the wavelength-swept laser, broadband vibration measurements become possible. Therefore, this method is anticipated to be applicable to a range of scenarios requiring rapid and multipoint measurements, such as assessing damage to objects [33], [34].

References

[1] J. M. Lopez-Higuera, *Handbook of Optical Fibre Sensing Technology*. Hoboken, NJ, USA: Wiley, 2002.

[2] A. Kersey et al., "Fiber grating sensors," *J. Lightw. Technol.*, vol. 15, no. 8, pp. 1442–1463, Aug. 1997.

[3] A. Othonos and K. Kalli, *Fiber Bragg Gratings*. Norwood, MA, USA: Artech House, 1999.

[4] E. J. Friebele et al., "Optical fiber sensors for spacecraft applications," *Smart Mater. Struct.*, vol. 8, no. 6, pp. 813–838, Dec. 1999.

[5] M. Majumder, T. K. Gangopadhyay, A. K. Chakraborty, K. Dasgupta, and D. K. Bhattacharya, "Fibre Bragg gratings in structural health monitoring—Present status and applications," *Sens. Actuators A, Phys.*, vol. 147, no. 1, pp. 150–164, Sep. 2008.

[6] V. R. Marrazzo et al., "Experimental tests of a full analog fiber optic monitoring system suitable for safety application at CERN," *IEEE Trans. Instrum. Meas.*, vol. 72, pp. 1–8, 2023.

[7] Q. Rong et al., "Ultrasonic imaging of seismic physical models using fiber Bragg grating Fabry–Pérot probe," *IEEE J. Sel. Topics Quantum Electron.*, vol. 23, no. 2, pp. 223–228, Mar. 2017.

[8] R. Ishikawa et al., "Pressure dependence of fiber Bragg grating inscribed in perfluorinated polymer fiber," *IEEE Photon. Technol. Lett.*, vol. 29, no. 24, pp. 2167–2170, Dec. 15, 2017.

[9] F. Yu, O. Saito, and Y. Okabe, "Laser ultrasonic visualization technique using a fiber-optic Bragg grating ultrasonic sensor with an improved adhesion configuration," *Struct. Health Monitor.*, vol. 20, no. 1, pp. 303–320, Jul. 2020.

[10] N. Sonoda, R. Takagi, I. Saito, T. Abe, S. Zhao, and Y. Tanaka, "Multipoint bending measurement using multicore fiber Bragg grating and two-photon absorption process in Si-APD," *IEEE Sensors J.*, vol. 21, no. 22, pp. 25736–25742, Nov. 2021.

[11] M. D. Todd, G. A. Johnson, and B. L. Althouse, "A novel Bragg grating sensor interrogation system utilizing a scanning filter, a Mach–Zehnder interferometer and a 3×3 coupler," *Meas. Sci. Technol.*, vol. 12, no. 7, pp. 771–777, Jul. 2001.

[12] C. G. Askins, M. A. Putnam, and E. J. Friebele, "Instrumentation for interrogating many-element fiber Bragg grating arrays," *Proc. SPIE*, vol. 2444, pp. 257–266, Apr. 1995.

[13] S. H. Yun, D. J. Richardson, and B. Y. Kim, "Interrogation of fiber grating sensor arrays with a wavelength-swept fiber laser," *Opt. Lett.*, vol. 23, no. 11, p. 843, Jun. 1998.

[14] R. Huber, M. Wojtkowski, and J. G. Fujimoto, "Fourier domain mode locking (FDML): A new laser operating regime and applications for optical coherence tomography," *Opt. Exp.*, vol. 14, no. 8, p. 3225, Apr. 2006.

[15] R. Huber, D. C. Adler, and J. G. Fujimoto, "Buffered Fourier domain mode locking: Unidirectional swept laser sources for optical coherence tomography imaging at 370000 lines/s," *Opt. Lett.*, vol. 31, no. 20, pp. 2975–2977, Oct. 2006.

[16] E. J. Jung et al., "Characterization of FBG sensor interrogation based on a FDML wavelength swept laser," *Opt. Exp.*, vol. 16, no. 21, p. 16552, Oct. 2008.

[17] T. Yamaguchi, K. Ishihara, and Y. Shinoda, "Field-programmable gate array-based multichannel measurement system for interrogating fiber Bragg grating sensors," *IEEE Sensors J.*, vol. 19, no. 15, pp. 6163–6172, Aug. 2019.

[18] T. Yamaguchi, W. Endo, and Y. Shinoda, "High-speed interrogation system for fiber Bragg gratings with buffered Fourier domain mode-locked laser," *IEEE Sensors J.*, vol. 21, no. 15, pp. 16659–16669, Aug. 2021.

[19] D. Huang, Y. Shi, F. Li, and P. K. A. Wai, "Fourier domain mode locked laser and its applications," *Sensors*, vol. 22, no. 9, p. 3145, Apr. 2022.

[20] K. Yuksel, V. Moeyaert, P. Mégret, and M. Wuilpart, "Complete analysis of multireflection and spectral-shadowing crosstalks in a quasi-distributed fiber sensor interrogated by OFDR," *IEEE Sensors J.*, vol. 12, no. 5, pp. 988–995, May 2012.

[21] M. Zhu and H. Murayama, "Fast demodulation of OFDR based long length FBG sensing system for noisy signals," *Opt. Exp.*, vol. 26, no. 16, pp. 19804–19814, Aug. 2018.

[22] T. Yamaguchi, M. Arai, and Y. Shinoda, "Development of wavelength measurement system of multiplex fiber Bragg gratings using optical frequency domain reflectometry," in *Proc. IEEE-ICST*, Auckland, New Zealand, May 2015, pp. 425–429.

[23] H. Jiang et al., "Wavelength detection of model-sharing fiber Bragg grating sensor networks using long short-term memory neural network," *Opt. Exp.*, vol. 27, no. 15, pp. 20583–20596, Jul. 2019.

[24] Y. C. Manie et al., "Enhancement of the multiplexing capacity and measurement accuracy of FBG sensor system using IWDM technique and deep learning algorithm," *J. Lightw. Technol.*, vol. 38, no. 6, pp. 1589–1603, Mar. 15, 2020.

[25] B. Li, Z. W. Tan, P. P. Shum, C. Wang, Y. Zheng, and L. J. Wong, "Dilated convolutional neural networks for fiber Bragg grating signal demodulation," *Opt. Exp.*, vol. 29, no. 5, pp. 7110–7123, Feb. 2021.

[26] M. A. Tefera, Y. C. Manie, C.-K. Yao, T.-P. Fan, and P.-C. Peng, "Meta-learning for boosting the sensing quality and utility of FSO-based multichannel FBG sensor system," *IEEE Sensors J.*, vol. 23, no. 24, pp. 31506–31512, Dec. 2023.

[27] T. Yamaguchi, H. Kawashima, H. Matsuda, and Y. Shinoda, "Experimental demonstration of peak wavelength measurement of multiplexing fiber Bragg gratings using convolutional neural network," *IEEE Sensors J.*, vol. 23, no. 9, pp. 9343–9352, May 2023.
[28] T. Yamaguchi, H. Kawashima, H. Matsuda, and Y. Shinoda, "Improvement of multiplexing capability of fiber Bragg gratings using convolutional neural network," in *Proc. OFS*, Naka-ku, Japan, 2023, p. 80.
[29] T. Ko, V. Peddinti, D. Povey, M. L. Seltzer, and S. Khudanpur, "A study on data augmentation of reverberant speech for robust speech recognition," in *Proc. IEEE Int. Conf. Acoust., Speech Signal Process. (ICASSP)*, New Orleans, LA, USA, Mar. 2017, pp. 5220–5224.
[30] Y. Li, H. Wang, L. M. Dang, A. Sadeghi-Niaraki, and H. Moon, "Crop pest recognition in natural scenes using convolutional neural networks," *Comput. Electron. Agricult.*, vol. 169, Feb. 2020, Art. no. 105174.
[31] D. R. Sarvamangala and R. V. Kulkarni, "Convolutional neural networks in medical image understanding: A survey," *Evol. Intell.*, vol. 15, no. 1, pp. 1–22, Jan. 2021.
[32] Z. Ouyang, J. Niu, Y. Liu, and M. Guizani, "Deep CNN-based real-time traffic light detector for self-driving vehicles," *IEEE Trans. Mobile Comput.*, vol. 19, no. 2, pp. 300–313, Feb. 2020.
[33] N. Takeda, Y. Okabe, J. Kuwahara, S. Kojima, and T. Ogisu, "Development of smart composite structures with small-diameter fiber Bragg grating sensors for damage detection: Quantitative evaluation of delamination length in CFRP laminates using Lamb wave sensing," *Compos. Sci. Technol.*, vol. 65, nos. 15–16, pp. 2575–2587, Dec. 2005.
[34] F. Yu, O. Saito, and Y. Okabe, "An ultrasonic visualization system using a fiber-optic Bragg grating sensor and its application to damage detection at a temperature of 1000 °C," *Mech. Syst. Signal Process.*, vol. 147, Jan. 2021, Art. no. 107140.

Tatsuya Yamaguchi (Member, IEEE) received the B.S., M.S., and Ph.D. degrees in engineering from Nihon University, Tokyo, Japan, in 2013, 2015, and 2018, respectively.

He then joined the Department of Electrical Engineering, Nihon University. His current research interests include optical measurements, digital signal processing, structural health monitoring, and optical fiber sensing.

Dr. Yamaguchi is a member of the Institute of Electrical Engineers of Japan (IEEJ) and the Society of Instrument and Control Engineers (SICE).

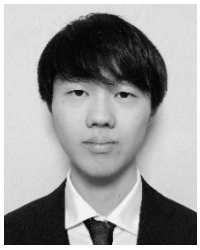

Hiroto Kawashima received the B.S. and M.S. degrees in engineering from Nihon University, Tokyo, Japan, in 2022 and 2024, respectively.

He is with Tokyo Electric Power Company. His current research interests include optical fiber sensing.

Hiroki Matsuda received the B.S. and M.S. degrees in engineering from Nihon University, Tokyo, Japan, in 2022 and 2024, respectively.

He is with Central Japan Railway Company. His current research interests include optical fiber sensing.

Yukitaka Shinoda (Member, IEEE) received the B.Sc., M.Sc., and Ph.D. degrees in electrical engineering from Nihon University, Tokyo, Japan, in 1987, 1989, and 2004, respectively.

He was a Visiting Researcher at Virginia Polytechnic Institute and State University (Virginia Tech), Blacksburg, VA, USA, from 2009 to 2010. Since 2012, he has been a Professor at the College of Science and Technology, Nihon University. He has focused on laser sensing, digital signal processing, motion analysis, and optical scanning holography.

Dr. Shinoda is a member of the Institute of Electrical Engineers of Japan (IEEJ), the Society of Instrument and Control Engineers (SICE), and Japan Society of Applied Physics (JSAP). He has been the Vice President of the Illuminating Engineering Institute of Japan (IEIJ) since 2023.